Physica A 533 (2019) 122051

Contents lists available at ScienceDirect

Physica A

journal homepage: www.elsevier.com/locate/physa

Modular structure in *C. elegans* neural network and its response to external localized stimuli

Carolina A. Moreira, Marcus A.M. de Aguiar *

Instituto de Física Física 'Gleb Wataghin', Universidade Estadual de Campinas, Unicamp 13083-970, Campinas, SP, Brazil

HIGHLIGHTS

- We probe the C. *elegans* neural network using the partially forced Kuramoto model.
- Stimuli were applied to topological, anatomical and functional modules.
- Response depends on stimulus intensity and inter-neuron connection strength.
- Topological and functional sets show patterns of correlation and anti-correlation.
- Modular structure hinders global synchronization.

ARTICLE INFO

Article history:
Received 19 February 2019
Received in revised form 13 June 2019
Available online 11 July 2019

Keywords:
Synchronization
C. elegans
Coupled oscillators
Kuramoto model
Neural networks
Modularity

ABSTRACT

Synchronization plays a key role in information processing in neuronal networks. Response of specific groups of neurons are triggered by external stimuli, such as visual, tactile or olfactory inputs. Neurons, however, can be divided into several categories, such as by physical location, functional role or topological clustering properties. Here we study the response of the electric junction *C. elegans* network to external stimuli using the partially forced Kuramoto model and applying the force to specific groups of neurons. Stimuli were applied to three topological modules, two ganglia, specified by their anatomical localization, and to the functional groups composed of all sensory and motoneurons. We found that topological modules do not contain purely anatomical groups or functional classes, corroborating previous results, and that stimulating different classes of neurons lead to very different responses, measured in terms of synchronization and phase velocity correlations. In all cases the modular structure hindered full synchronization, protecting the system from seizures. The responses to stimuli applied to topological and functional modules showed pronounced patterns of correlation or anti-correlation with other modules that were not observed when the stimulus was applied to a ganglion with mixed functional neurons.

1. Introduction

Understanding the network of neuronal connections in the brain is key to unravel the way it works and processes information. The complexity of these networks has been emphasized by many authors [1], and characterized with different measures, such as degree distribution, transitivity and betweenness centrality [2]. An important feature of neural networks is their high degree of heterogeneity, in the sense that the number of connections per neuron varies considerably and

* Corresponding author.
E-mail address: aguiar@ifi.unicamp.br (M.A.M. de Aguiar).

https://doi.org/10.1016/j.physa.2019.122051
0378-4371/

typically displays some sort of power law distribution. Moreover, neurons tend to form communities, where the density of connections is higher within than among communities. Because connections are constrained by anatomical features, neurons are also organized into physically arranged clusters, such as lobes or ganglia, where neurons with different functional roles coexist [3–5].

Communities are often related to specialized areas of the brain and their number and structure are an indication of how many different tasks it can perform [6]. The integration of communities, on the other hand, measures how well the outcomes of these different processes can combined to build a global view of the inputs [3]. When triggered by external stimuli, such as visual or olfactory inputs, the information processing occurs by the synchronized firing of neurons responsible to process those specific tasks [7,8]. Synchronization of larger sets of neurons, or even global synchronization, indicates cerebral disorders [9] such as epilepsy [10] and Alzheimer's disease [11], causing a general breakdown in the neuronal network. Lack of synchronization, on the other hand, suggests difficulty to respond to the stimulus or to function properly, as reported in unsuccessful overnight memory consolidation in old people [12], deficiency in the auditory-motor connections [13] or brain disorders in autistic individuals [14,15]. In this context, the knowledge of the organization of different types of neurons in the network and their segregation into modules or communities is fundamental to understand how stimuli affect the target module and under what conditions it propagates to other regions leading to global or poor responses.

In this work we probe the community structure of the neural electrical junction network of the *C. elegans* using the partially forced Kuramoto model of synchronization [16]. We aim to understand how the network responds to external localized stimuli and which modules are more affected when a specific group of neurons, that can be a functional group or a physically arranged module, is stimulated. We use two different metrics to characterize the overall behavior of the network under a localized stimulus: the synchronization of neurons within and between modules, as measured by the usual Kuramoto order parameter, and the phase-velocity inter-neuron correlation. We want to investigate the behavior of the system as a function of parameters such as stimulus intensity and inter-neuron connection strength. In particular we are interested in cases leading to global induced synchronization and highly correlated behavior, where the network responds as a whole, or to uncorrelated states, where neurons do not react to each other. Our simulations are guided by the results of a previous paper [16] where we studied the partially forced Kuramoto model on synthetic networks, using the external force to simulate a localized stimulus.

C. elegans is a nematode animal, unsegmented and with bilateral symmetry, exhibiting physiological similarity to mammals as regards the nerves and neurotransmitters morphologies and it is considered a model organism in studies of disorders related to human nervous system, such as epilepsy [17,18] and Parkinson's disease [19,20]. It was the first multicellular animal to be its whole nervous system mapped, containing only 302 neurons. Its neural network has a huge data with open source, such as the WormAtlas [21] and the OpenWorm [22]. Because it is a real complex network, we choose this small neural network, extracting all necessary data from WormAtlas.

The 248 neurons of the electrical junction network are anatomically classified as belonging to head, body or tail, and neuron types are divided into motoneurons, interneurons and sensory neurons. We have also performed a classification into 10 ganglia (A: anterior ganglion, B: dorsal ganglion, C: lateral ganglion, D: ventral ganglion, E: retrovesicular ganglion, F: posterolateral ganglion, G: ventral cord neuron group, H: pre-anal ganglion, J: dorsorectal ganglion, K: lumbar ganglion [21]) which is a finer division of the anatomical one.

The network is first decomposed into three modules based on topological properties and numbered by 1, 2 and 3 from largest to smallest. This modularization procedure was made on software Cytoscape using the app ModuLand [23,24]. Each module contains neurons from the three anatomical parts, and consequently the 10 ganglia, and of the three types. We applied the stimulus to the largest module, then on the ganglion C and finally to the sensory neurons and then we observe the response of other neurons. We show that no single partition of the brain into communities can account for its behavior under stimuli. All partitions analyzed here, topological, anatomical and functional, play a role in the response to external localized stimuli, revealing the complexity of the brain's wiring and function.

This paper is organized as follows: in Section 2 we describe the materials and methods, showing the partially forced Kuramoto model, the *C. elegans* neural connectome and the order parameters used to measure the state of the network. The results of numerical calculations and its analysis are in Section 3. Finally, we summarize our discussion in Section 4.

2. Materials and methods

2.1. Partially forced Kuramoto model

The Kuramoto model of coupled oscillators [25] is a paradigm in the study of synchronization and has been explored in connection with biological systems, neural networks and the social sciences [26,27]. Here we consider a modified version of the original Kuramoto model where each oscillator interacts only with a subset of the other oscillators, as specified by a network of connections [28]. Moreover, part of the oscillators also interacts with an external periodic force [16,29–31]. The force can be interpreted as an external stimulus and the set of oscillators coupled to it represents the 'interface' of the system, like the photo-receptor cells in the eye [8]. The oscillators are described by their phase θ and system is governed by the equations [16]

$$\dot{\theta}_i = \omega_i + F\,\delta_{i,C}\,\sin(\sigma t - \theta_i) + \frac{\lambda}{k_i}\sum_{j=1}^{N} A_{ij}\sin(\theta_j - \theta_i), \tag{1}$$

where N is the number of oscillators, λ is the internal coupling strength, A_{ij} is the adjacency matrix of internal connections; $k_i = \sum_j A_{ij}$ is the degree of node i; F and σ are respectively the amplitude and frequency of the external force; and C is the subgroup of oscillators subjected to the external force. We have also defined $\delta_{i,C} = 1$ if $i \in C$ and zero otherwise and we shall call N_C the number of oscillators in the set C. The natural frequencies ω_i are taken from a distribution $\rho(\omega)$, which is here chosen to be Gaussian with zero average and width 1.0.

Following [31] we define

$$\phi_i = \theta_i - \sigma t. \tag{2}$$

In these new variables the explicit time dependence disappears and the equations become

$$\dot{\phi}_i = \omega_i - \sigma - F\,\delta_{i,C}\sin\phi_i + \frac{1}{k_i}\sum_{j=1}^{N}\lambda_{ij}\sin(\phi_j - \phi_i), \tag{3}$$

where $\lambda_{ij} = \lambda A_{ij}$.

The adjacency matrix A_{ij} gives the strength of interaction between oscillators i and j. For unweighted networks A_{ij} assumed the value 1 if they interact and 0 otherwise, but weighted networks like that of the *C. elegans*, might have very inhomogeneous distributions of weights. For networks that can be divided into anatomical or functional communities, the external force can be applied to one of the communities as a way to probe its influence on the others. Thus, we will investigate how the control parameters, λ and F, affect the spontaneous and induced synchronization of the focal community (where the force is applied) and how it spreads to the other communities of the system.

If there is no external force and if the internal coupling constant λ is sufficiently large the oscillators synchronize spontaneously with frequency $\bar{\omega} = \sum \omega_i/N$ in the original coordinates θ or with frequency $\bar{\omega} - \sigma$ in the rotating frame ϕ. On the other hand, if both λ and F are large the system synchronizes with the external frequency σ in the original frame or $-\bar{\omega}$ in the rotating frame. In our simulations, since the Gaussian distribution is symmetric, $\bar{\omega} = 0$, the spontaneous synchronization corresponds to global frequency $\dot{\psi} = -\sigma$ and forced synchronization to frequency $\dot{\psi} = 0$ [16].

Following [16] we can estimate the minimum intensity of the external force, F_c, required to induce global synchronization using the relation

$$F_c = \frac{\sigma}{f}\frac{\langle k\rangle}{\langle k\rangle_C}, \tag{4}$$

where $f = N_C/N$ is the fraction of forced neurons; $\langle k\rangle$ and $\langle k\rangle_C$ are the average degree of the network and the forced module, respectively.

2.2. Modularization

Understanding how connections are arranged in neural networks is key to understand how the brain functions and transmits information [32–34]. Neurons can be grouped by their location in the brain, by their function and also by their connectivity with other neurons, independently of their position or function. Networks can generally be decomposed into these *topological* modules, also called clusters or communities, where a large number of links join nodes of the same module and comparatively few links join nodes belonging to different modules. Several methods have been recently proposed to detect modules, each providing a different decomposition, and no optimal algorithm has yet been devised [35]. The strength of each decomposition, however, can be measure by the modularity coefficient [36,37]

$$Q_w = \frac{1}{2m}\sum_{i,j}\left(A_{ij} - \frac{k_i k_j}{2m}\right)\delta(c_i, c_j), \tag{5}$$

where A_{ij} is the (weighted) adjacency matrix, k_i is the sum of the weights of all links attached to node i, c_i is the module of node i, $\delta(c_i, c_j) = 1$ if nodes i and j belong the same module and $2m$ is the sum of all of the link weights in the network. Eq. (5) gives $Q_w = [-0.5, 1.0]$, where positive values indicate that there exist a larger number of connections between nodes of the same community than if connections were made randomly, and negative values mean less intra-module connections. For real complex networks, $0.3 < Q_w < 0.7$ [36,37]. For unweighted networks the same formula can be used, replacing k_i by the degree of node i and m by the total number of links in the network.

Previous analysis of neural networks have shown that they do exhibit modular organization [35,37]. The most common algorithms for module detection in biological network analysis are the so called hierarchical clustering [35]. This technique is classified in two types: in the first, individual neurons are initially grouped if they have high similarity; then these groups are further clustered together and so on until the desired number of modules is formed (bottom up, agglomerative algorithm). In the second type of algorithm the network is divided in groups by the removing links that connect nodes with low similarity (top down, divisive algorithm).

In this work we used the ModuLand plug-in [23,24] of the software Cytoscape [38] to study the modularization of the *C. elegans* network. This tool uses a hierarchical algorithm which detects multiple layers of communities, where nodes of the higher hierarchical step are modules of the lower step. ModuLand was tested in biological systems, such as protein structure and metabolic networks, providing modules which correspond to relevant biological communities [23,24]. For

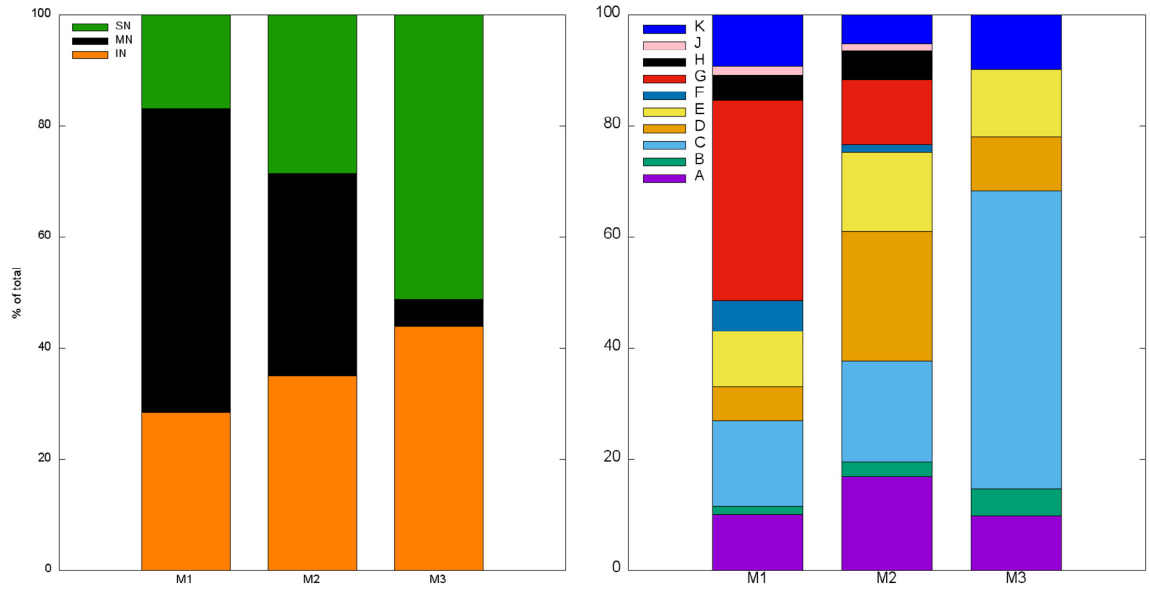

Fig. 1. Histograms representing the fraction of (left) neuronal class (SN: sensory neuron, MN: motoneuron and IN: interneuron) and (right) of ganglia (A: anterior ganglion, B: dorsal ganglion, C: lateral ganglion, D: ventral ganglion, E: retrovesicular ganglion, F: posterolateral ganglion, G: ventral cord neuron group, H: pre-anal ganglion, J: dorsorectal ganglion, K: lumbar ganglion) for each module (M_1: module 1, M_2: module 2 and M_3: module 3).

the present case of the *C. elegans* electric junction network ModuLand divided the network into 3 modules with $Q_w = 0.47$. Other procedures result in different partitions; for example [5] obtained 6 modules with $Q_w = 0.375$, [39] found 5 modules with $Q_w = 0.49$ and [40] divided the network into 11 and 15 modules with $Q = 0.63$ and $Q_w = 0.66$, respectively. They all used slightly different versions of the *C. elegans* network, including or excluding some neurons. Here we focused on the case of 3 modules to compare with the 3 functional categories (motor, sensory, interneurons) and 3 major anatomical classes (head, midbody, tail). Further information is summarized in table I of S.M. We have also considered two other partitions, containing 5 and 10 modules respectively. The details are described on S.M. (Section 2).

2.3. C. elegans neural connectome

Based on structural and functional properties of the neural network of *C. elegans*, Varshney et al. [41] and Yan et al. [42] presented a division of neuronal classes, totalizing 118, in three categories: sensory neurons (SN), which respond to environmental variations, motoneurons (MN), recognized by the presence of neuromuscular junctions and responsible by locomotion, and the interneurons (IN), which cover all of other classes. The adjacency weighted matrix is defined as follows: the element w_{ij} represents the total number of synapses interchange between the pair of neurons *ij*. In [41] the authors also divide the set into the gap junction network, which refers to the electrical synapses, and the chemical synapses network.

Gap junctions are a medium for electrical coupling between neurons and, since the electric signal can be made in both directions, the electrical junction network is considered undirected and, consequently, its adjacency matrix symmetric. On the other hand, the chemical synapses network is a directed and weighted network, whose adjacency matrix is asymmetric. Here we will concentrate on the electrical junction network only.

We analyzed the gap junctions neural network of nematode *C. elegans* extracting the data from WormAtlas [21]. The full connectome has 279 neurons (nodes) and 514 gap junctions (connections) divided into a giant component with 248 neurons plus 31 neurons not connected with it. Here we will study the dynamics on the giant component. Thereby, we built the weighted electrical junction (EJ) network of the *C. elegans* with 248 neurons and 511 gap junctions. We also used a hierarchical algorithm to detect communities on the EJ network. For that, we used the package ModuLand [23,24] available on the free software Cytoscape [38]. The algorithm provided three modules (M_1, M_2, M_3) with modularity $Q_w = 0.47$.

Each neuron were further classified as belonging to one of three functional categories (sensory, motor and interneurons) and one of the 10 ganglia (A: anterior ganglion, B: dorsal ganglion, C: lateral ganglion, D: ventral ganglion, E: retrovesicular ganglion, F: posterolateral ganglion, G: ventral cord neuron group, H: pre-anal ganglion, J: dorsorectal ganglion, K: lumbar ganglion [21]). The compositions of neuronal categories and ganglionic classification in each module are shown in Fig. 1. The ganglia are a finer division of the anatomical classification into head (H), body (B) and tail (T). The histograms in Fig. 2 summarize the information extracted from the WormAtlas showing how ganglia are distributed physically (left panel) and how neuronal functions are represented in each ganglion (right panel). Note that ganglia A, B, C and D belong to the head, G is entirely localized in the body and J and K belong to the tail.

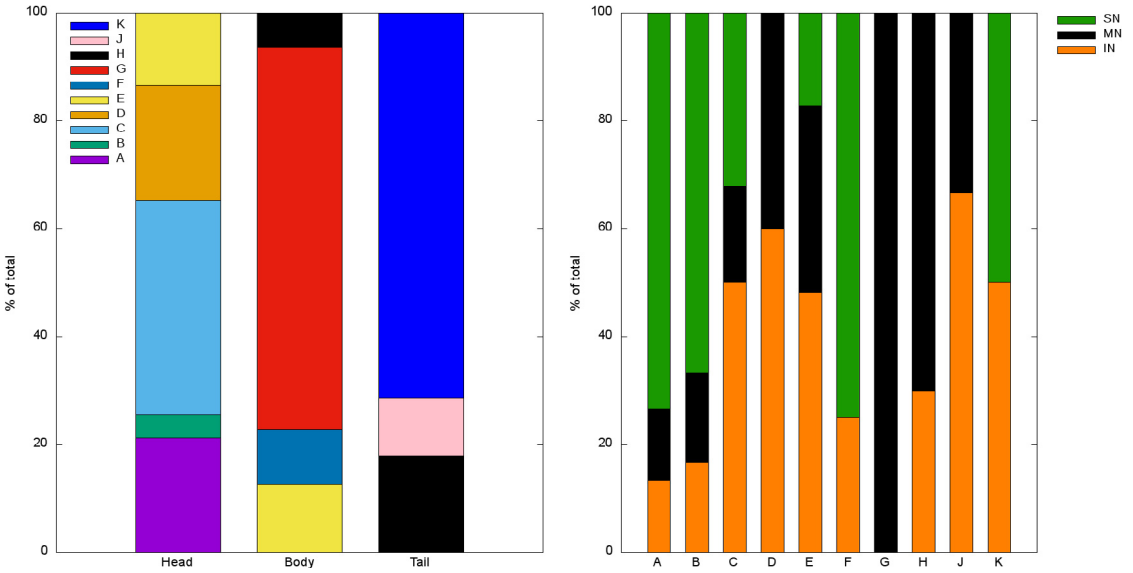

Fig. 2. Histograms representing the fraction of (left) different ganglia distributed by physical localization (head, midbody and tail) and (right) the fraction of classes (SN, MN and IN) component in each ganglion.

This set of divisions of the neural network into communities can be classified as (i) topological (M_1, M_2, M_3); (ii) anatomical (by ganglion A-K) and; (iii) functional (SN, MN, IN). They are all different and intertwined, showing the complexity of the EJ network.

In the next section we will apply the stimulus to M_1 (the largest of the topological modules), to ganglion C (completely located in the head and with mixed types of functional neurons) and to the sensory neurons. Results for modules M_2, M_3, ganglion G and motoneurons are shown in the supplementary material. Previous works [40] have shown that ganglion C is important in the transmission of information between neurons that receive sensory stimulus and those responsible for motor processing. We also performed simulations on ganglion G (see S.M.), which is localized completely in the midbody (Fig. 2 left) and is composed only by motoneurons (Fig. 2 right). Finally we note that the sensory neurons are responsible for collecting information from external environment and react to stimuli inside the organism, acting as a input channel. In this sense, *C. elegans* uses these neuronal functions to explore the ambient, navigating over thermal, chemical and oxygen variations, in addition to avoid hostile behavior [21].

2.4. Order parameters and correlations

The partially forced Kuramoto dynamics will be applied to the *C. elegans* as a way to probe its modular structure. Forcing a particular module may or may not induce synchronization with the external frequency on other modules of the system. In order to monitor the behavior of separate modules we define

$$z_n = \frac{1}{N_n}\sum_{i\in M_n} e^{i\phi_i} \equiv r_n e^{i\psi_n} \tag{6}$$

where the subscript n specifies the module M_n of size N_n. Therefore, r_n is a local order parameter that measures how much the oscillators in the module are synchronized among themselves. The angular velocity $\dot{\psi}_n$ provides information about the motion of the set: $\dot{\psi}_n = 0$ implies sync with the external force, $\dot{\psi}_n = -\sigma$ refers to spontaneous sync whereas nonconstant values indicate more complex behavior.

Intermodule behavior will also be monitored by the quantities

$$z_{nm} = \frac{1}{N_n + N_m}\sum_{i\in M_n\cup M_m} e^{i\phi_i} \equiv r_{nm} e^{i\psi_{nm}} \tag{7}$$

with similar interpretations. Finally we compute the usual order parameter

$$z = \frac{1}{N}\sum_{i=1}^{N} e^{i\phi_i} \equiv r_t e^{i\psi_t} \tag{8}$$

that provides information on the global network synchrony.

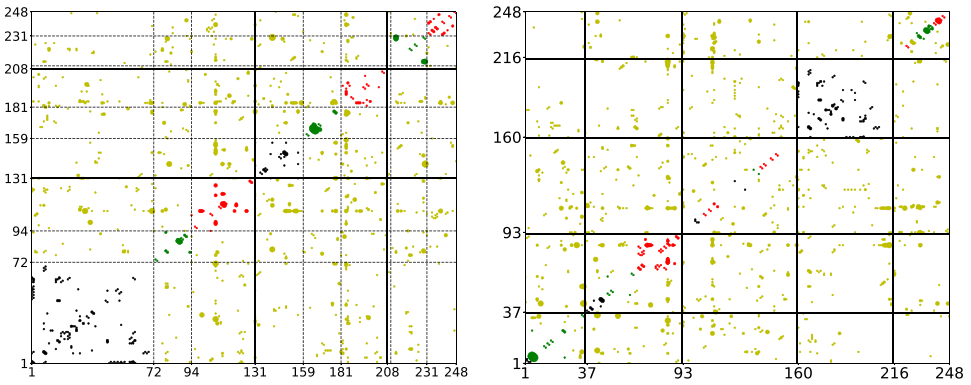

Fig. 3. Left panel: weighted adjacency matrix highlighting the 3 topological modules M_1, M_2 and M_3 separated by thick black lines and subdivided into motor (black), sensory (green) and interneurons (red) by dashed black lines. Intermodule connections are shown in yellow. Right panel: weighted adjacency matrix highlighting 5 groups of ganglia separated by thick black lines, {A, B}; {C}; {D, E, F}; {G} and {H, J, K}. Subdivisions and intermodule connections follow the functional colors of left panel.

Velocity–velocity correlations between all pairs of oscillators are defined by

$$\tilde{c}(i,j) = \frac{1}{T}\int_{t_0}^{t_0+T} (\dot{\phi}_i(t) - \langle\dot{\phi}_i\rangle)(\dot{\phi}_j(t) - \langle\dot{\phi}_j\rangle)\, dt \tag{9}$$

where

$$\langle\dot{\phi}_i\rangle = \frac{1}{T}\int_{t_0}^{t_0+T} \dot{\phi}_i(t)\, dt \tag{10}$$

and t_0 is a sufficiently long time so that the transient dynamics has passed.

The normalized velocity–velocity correlation function is then defined as:

$$c(i,j) = \frac{\tilde{c}(i,j)}{\sqrt{\tilde{c}(i,i)\,\tilde{c}(j,j)}}, \tag{11}$$

where $|c(i,j)| \leq 1$. We note that the correlation is computed in terms of the fluctuations of the average velocity, that was subtracted out in Eq. (9). The 248×248 correlation matrix gives direct information about the effect of one neuron over another, irrespective of their synchronization state. If an increase in the velocity of i leads to the average increase in the velocity of j then nodes i and j are positively correlated and $c(i,j) > 0$. If, on the other hand the velocity of j decreases, they are negatively correlated and $c(i,j) < 0$. Finally, if they are uncorrelated $c(i,j) \approx 0$. In the simulations we used $t_0 = T/2$ and $T = 20$ which was enough for the equilibration of the system.

The parameters z_n provide information about the synchronization of each module, whereas the average value of the phase velocity $\dot{\psi}_n$ tells whether the module follows the external force or spontaneous collective motion. This information is complemented by the velocity–velocity correlation, which measures the effect of one node over the other even if they synchronize with different frequencies or are not synchronized at all.

3. Results

Fig. 3 shows the weighted adjacency matrix ordered according to the topological modules M_1, M_2 and M_3 (left panel). Modules are separated by thick black lines and subdivided into motoneurons (black), sensory neurons (green) and interneurons (red) by dashed black lines. The size of the dot is proportional to the intensity A_{ij} and intermodule connections are represented in yellow. The right panel shows the adjacency matrix ordered by ganglion, from head to tail. The thick black lines highlight 5 groups of ganglia: {A, B}; {C}; {D, E, F}; {G} and {H, J, K}. These groupings were defined to facilitate the visualization of the plots and to emphasize the forced ganglia (ganglion C in Fig. 5 and ganglion G in figures 7 and 8 in the supplementary material). Subdivisions and intermodule connections follow the functional colors of left panel. The indexes in both panels delimit the divisions made.

In order to analyze the interdependencies of the modules for different partitions of the EJ network, we have simulated the application of an external stimulus to one of the modules and observed its effect on the others. The stimulus is modeled by an external periodic force acting only on the selected module under the Kuramoto dynamics as described in Section 2.1. In all our simulations we have fixed $\sigma = 3$. The effects on the other modules is measured by local order parameters, such as r_{nm}, and the normalized velocity–velocity correlation function as described in Section 2.4. Here we show the numerical results for the cases where the stimulus was applied only to M_1, or to ganglion C or to the sensory

Table 1
Basic properties of forced modules: number of neurons, fraction of nodes, average degree and theoretical critical force for full synchronization.

	Module 1	Ganglion C	Sensory neurons	Network
Number of neurons	$N_{M_1} = 130$	$N_C = 56$	$N_{SN} = 65$	$N = 248$
Fraction of nodes	$f_{M_1} = 52.42\%$	$f_C = 22.58\%$	$f_{SN} = 26.21\%$	$f = 100\%$
Average degree	$\langle k_{M_1} \rangle = 7{,}96$	$\langle k_C \rangle = 10{,}16$	$\langle k_{SN} \rangle = 5{,}27$	$\langle k \rangle = 7{,}13$
Critical force (Eq. (4))	$F^{M_1}_{c,theo} = 5{,}12$	$F^{C}_{c,theo} = 9{,}32$	$F^{SN}_{c,theo} = 22{,}96$	$F_{c,theo} = 3{,}00$

neurons, Figs. 4–6, respectively. In all cases we show the global (r_t) and local (r_{nm}) order parameters as a function of the intensity F of the external force for four values of the internal coupling λ, panels (a) to (d), and the velocity–velocity correlation matrices in panels (e) to (t).

We used equation (4) to calculate the expected critical force to induce global synchronization in an equivalent random network. The values of the fraction f of forced nodes, the average degree $\langle k \rangle_C$ of the forced set and that of the whole network $\langle k \rangle$ are summarized in Table 1. In Ref. [16], fully synchronized states were defined by the conditions $r_t > 0.95$ and $|\dot{\psi}_t| < 0.01$. Here we also classify the network as *partially synchronized* if $0.8 < r_t \leq 0.95$ and $|\dot{\psi}_t| < 0.1$. Further information can be found in table II of S.M.

Stimulating the M_1: the role of topology

Fig. 4 shows the results of simulations when only the neurons of M_1 are forced (indexes 1 to 130 in the left panel of Fig. 3.) As F increases, the neurons go through a region of asynchrony around $F = 5$, which is close to theoretical value for full synchrony $F^{M_1}_{c,theo} = 5.12$ calculated with Eq. (4), and then they synchronize with the external force ($\dot{\psi}_{M_1} = 0$, Fig. 1 on S.M.) for F larger than about 10, where $r_{M_1} \to 1$. For large internal coupling λ, all modules appear to synchronize with external force (see panel (d) of Fig. 4 and panel (l) of Fig. 1 on S.M.), but M_3 has large fluctuations in $\dot{\psi}_{M_3}$ (panel (p), Fig. 1 on S.M.). The global order parameter reaches its maximum value at $r_t \approx 0.9$ with $\dot{\psi}_t \approx 0.0$ for $\lambda = 100$ (Tables 2 and III of S.M.).

The most striking feature of these simulations is the strong anti-correlation patterns developed between M_1 and M_2 for $\lambda \leq 20$. From the top panels we notice that, in these cases, M_1 is in synchrony with the external force whereas M_2 is still synchronized spontaneously. Nevertheless the effects of M_1 over M_2 are very clearly shown by the purple areas of the correlation plots. This indicates a lower value of the inter-modules order parameter r_{nm}, as can be seen between M_1-M_2 and M_2-M_3 (panel (k) on Fig. 4 and Fig. 1 on S.M.). On the other hand, the presence of positive correlations between M_1 and M_3 (panel (q) on Fig. 4), is accompanied by an increase of r_{13}.

Stimulating ganglion C: the role of anatomy

Fig. 5 shows the results of simulations when ganglion C is forced. The behavior of the order parameters r_t and r_n as a function of F is similar to that observed when forcing the neurons of M_1, exhibiting a region of asynchrony between $F = 5$ and $F = 10$, which contains the theoretical value, $F^{C}_{c,theo} = 9.32$, followed by stabilization for larger F. The forced neurons are clearly seen as a bright yellow blocks in panels (e) to (h).

For sufficiently large F ganglion C synchronizes with the external force ($r_2 \to 1$, panels (a) to (d), and $\dot{\psi}_2 = 0$, Fig. 4 on S.M.) for all values of λ considered. However, the velocity–velocity correlation matrices show much simpler patterns, displaying either nearly complete correlation (yellow areas in panels (g), (h), (k), (l) and (p)), or almost no correlation at all (large red areas in panels (i), (m), (n), (q) and (r)) with ganglion C itself showing reduced internal correlations. Even for $F > 12$, where r_2 indicates that C is nearly fully synchronized for all λ's, the correlation matrices show regions of mixed behavior, especially for small λ, which means that part of neurons of C are non-correlated with each other or even anti-correlated (see also Fig. 4, panels (a), (b), (i) and (j) on S.M.). Although all ganglia seem to synchronize with the external force for $\lambda \geq 40$ and $F > 12$, their dynamics are uncorrelated with other ganglia. The only exception is ganglion G, that shows up as a yellow square in the plots (see also Figs. 7 and 8 of S.M.).

We also note that for $\lambda = 40$ the motor part of ganglion C (small yellow squares indexed by 37 to 46) correlates separately from the rest of C for $F = 12$, panel (o), and $F = 17$, panel (s), which means that motoneurons respond differently to external stimuli. For $F = 17$, panels (q), (r), (s) and (t), the number of correlated neurons increases from $\lambda = 10$ to $\lambda = 40$ but for $\lambda = 100$ the entire network goes out of phase, with the exception of ganglion G: it keeps its internal correlation at all times, maybe because it is entirely a motor ganglion type. Note that $r_4 \approx 1$ only for $\lambda = 100$, panel (d), which means that full sync requires large internal coupling. We also note that the global order parameters for $\lambda = 100$ are $r_t = 0.98$ and $\dot{\psi}_t = 0.0$ (Table 2 and VI of S.M.), which means that the network is fully synchronized.

Stimulating the sensory neurons: the role of function

Fig. 6 shows the numerical results when all sensory neurons (SN) receive the external stimuli. Panels (a) to (d) show that the behavior of the network is more complex in this case. The SN synchronize with the external force for: (*i*) $\lambda = 10$ and $F > 10$ (panels (a), (i) and S.M. Fig. 7), (*ii*) $\lambda = 20$ and $F > 15$ (panels (b), (j) and S.M. Fig. 7), (*iii*) $\lambda = 40$ and $F > 20$ (panels (c), (k) and S.M. Fig. 7) and (*iv*) $\lambda = 100$ and $F > 30$ (panels (d), (l) and S.M. Fig. 9). In (*iii*) and (*iv*) the values of F are close to the theoretical value $F^{SN}_{c,theo} = 22.96$. Contrary to all other cases, larger values of λ hinders the synchronization

Table 2
Global order parameters for each forced subset of neurons. The network is considered to be partially synchronized if $0.8 < r_t \leq 0.95$ and fully synchronized if $r_t > 0.95$ and $\dot{\psi}_t < 10^{-2}$.

λ	r_{t-M_1}	$\dot{\psi}_{t-M_1}$	Global sync (M_1)	r_{t-C}	$\dot{\psi}_{t-C}$	Global sync (C)	r_{t-SN}	$\dot{\psi}_{t-SN}$	Global sync (SN)
10	0.55	0.07	No	0.52	0.03	No	0.59	−2.84	No
20	0.54	−0.01	No	0.67	0.00	No	0.63	−2.46	No
40	0.65	0.05	No	0.87	0.00	Partial	0.54	−2.70	No
100	0.91	0.02	Partial	0.98	0.00	Yes	0.81	0.00	Partial

of the forced group, since r_{SN} decreases from $\lambda = 10$ to $\lambda = 100$, although $\dot{\psi_{SN}} = 0$ (Fig. 7, S.M.). For $\lambda = 100$, the global order parameters are $r_t \approx 0.81$ and $\dot{\psi}_t = 0.0$ (Table 2 and VIII of S.M.), thus the system synchronizes only partially.

For $\lambda \leq 40$, the motoneurons and almost half of interneurons were in spontaneous sync (panels (a), (b), (i) and (j) on Fig. 7, S.M.), while for $\lambda > 40$ and $F > 30$ most neurons were synchronized with external stimuli. The velocity–velocity matrices also show regions of anti and non-correlation, as can be seen on purple and red areas of Fig. 6, respectively, particularly for weak internal coupling, $\lambda < 40$. In these cases, the lack of correlation seems to indicate a lower value of inter-modules order parameter r_{nm}, as can be seen in panels (e) to (h) of Fig. 9 on S.M.

4. Discussion

Information processing in the brain requires the synchronous firing of specific groups of neurons to respond to external stimuli [43–45]. In the retina, neighboring cells synchronize at a very fine timescale to keep up with the constant motion of the eyes and the head [46,47] and information about visual stimuli is contained in the relative spike timing [48]. In the auditory system, sound localization is determined by phase locking in the auditory nerve fibers [49], producing correlations in spike timing that encodes the physical location of the sound source [50]. Although synchronization is ubiquitous in neural systems [43] the specific group of neurons that synchronize depends on the type of stimulus and the time scale of the synchronization might vary from milliseconds [48] to rates up to 170 spikes per second [49].

Groups of neurons can be defined in many ways, taking into account their anatomical location, their functional role or their topological properties in the network. In this paper we investigated the importance of these divisions as targets to stimuli, as well as their roles in spreading the inputs to other parts of the brain. Here we used a much simplified model of synchronization given by the Kuramoto system of phase oscillators subjected to a single stimulus, described by the external force, applied only to a subset of neurons representing a topological module (Fig. 4), a ganglion composed of different functional neurons (Fig. 5) or the sensory neurons (Fig. 6). Because the stimulus is permanently turned on in the model, the system behavior converges to an oscillatory state corresponding to an infinite sequence of spikes, which is clearly a simplification. However, the model does provide interesting information about the ability of the group of neurons receiving the input to synchronize among themselves or with other groups, or to develop correlations.

The modularization procedure applied to EJ network reveals that topological modules do not contain purely anatomical groups or functional classes, but mixes neurons belonging to different ganglia and functional classes. This is illustrated in Fig. 1, where we have analyzed the distribution of neuronal classes and ganglia membership in each module. This corroborates previous studies that employed different modularization techniques [5,39–41,51] and highlights the complexity of the neuronal wiring regarding their location and function. The response of the electrical neural network to the stimulus was different for each type of neuron grouping, as we summarized in Table 2 in terms of synchronization and below in terms of cross correlations with other modules.

Stimulation of the neurons of the largest topological module M_1 induced strong anti-correlation in the velocity fluctuations of the neurons in M_2 and M_3 (purple areas of panels (i), (j) and (m) on Fig. 4 or between M_2 and M_3 (panel (k) on the same figure), which kept their original state of spontaneous synchronization for moderate values of the internal coupling constant λ. The smallest topological module M_3 remained oblivious to the stimulus even for large values of λ. Interestingly, for intermediate values of the forcing (panel (j) on Fig. 4), the neurons of M_1 became mostly uncorrelated (red areas on Fig. 4), indicating a parameter region of poor response to the stimulus. It is possible, however, to identify the modular structure by the presence of three blocks, each of one corresponding to M_1, M_2 and M_3. A very similar behavior is observed when M_2 is stimulated (Figs. 2, 3 and table IV of the S.M.). When the stimulus is applied to M_3, however, it never spreads to the other modules, which remain in spontaneous synchrony but develop a pattern of anti-correlation inter-modules for sufficiently large values of λ and F (Figs. 4. 5 and table V of S.M.).

The response of the network to stimulation of ganglion C was quite different from that of M_1 displaying essentially two distinct regions with (I) large parameter intervals of almost complete uncorrelated behavior, which occurs for $\lambda \leq 20$ (red areas on panels (i), (m), (n), (q), (r) and (t) on Fig. 5) and (II) complete correlated behavior, with $\lambda \geq 40$ (yellow areas on Fig. 5). Effective synchronization of ganglion C with the external force required large values of the coupling constant. Contrary to what occurs when forcing the topological module, the blocks of the correlation matrix corresponding to ganglia groups cannot be clearly distinguished, except for ganglion G (Figs. 4 and 5 on S.M.), which seems to hold high correlation between its neurons, possibly because it is the only group entirely composed by one class (motoneurons). Stimulation of ganglion G is presented in the S.M. Figs. 7, 8 and table VII. The patterns of anti-synchronization between modules are

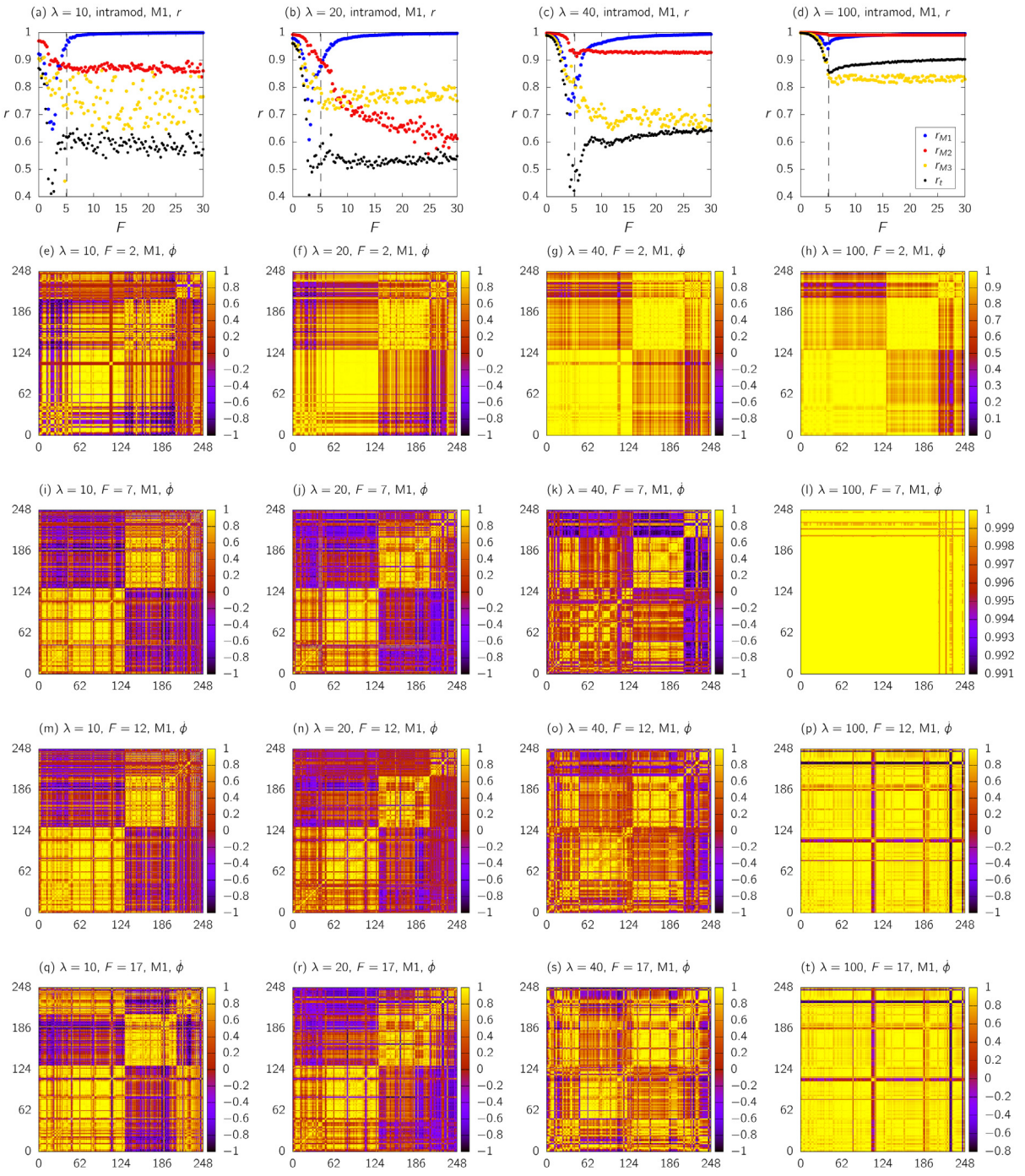

Fig. 4. Panels (a)–(d): the global and local order parameters as a function of the external force F acting on neurons of M_1 for λ fixed. The dashed lines indicate the critical force, $F_{c,theo}^{M_1} = 5.12$. Panels (e)–(t): the velocity–velocity correlation matrix 248 × 248 obtained using Eq. (11). In each panel, the fixed parameters λ and F are indicated. The M_1 neurons are indexed by 1 to 130, the M_2 neurons by 131 to 207 and the M_3 neurons are indexed by 208 to 248.

again observed in this case, reinforcing the idea that functionality, not spatial location, is the relevant structure in this case.

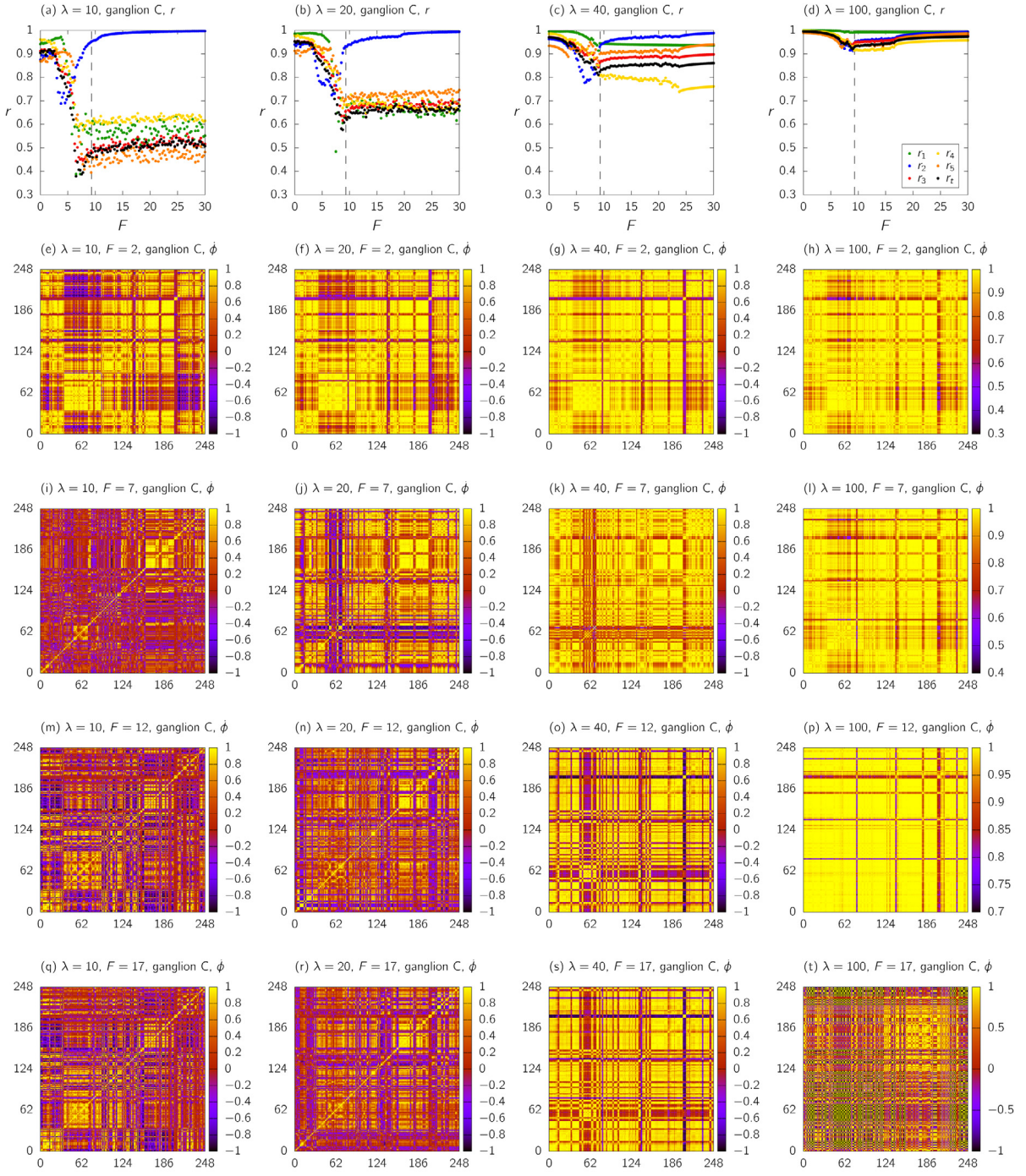

Fig. 5. Panels (a)–(d): the global and local order parameters as a function of the external force F acting on ganglion C for λ fixed. The dashed lines indicate the critical force, $F^{C}_{c,theo} = 9.32$. Panels (e)–(t): the velocity–velocity correlation matrix 248 × 248 obtained using Eq. (11). In each panel, the fixed parameters λ and F are indicated. The group 1 ({A,B}) are indexed by 1 to 36, group 2 ({C}) by 37 to 92, group 3 ({D, E, F}) by 93 to 159, group 4 ({G}) by 160 to 215 and group 5 ({H, J, K}) are indexed by 216 to 248.

Finally, stimulation of the sensory neurons leads to synchronization with the external driving for $\lambda \leq 40$, while the other two functional classes remained in spontaneous sync. It was only with strong internal coupling, $\lambda > 40$, and force larger than the theoretical value, $F > 30$, that most of neurons were induced to the forced sync. The results also show many regions of anti and non-correlation (purple and red areas on Fig. 6, respectively). Matrix blocks of similar

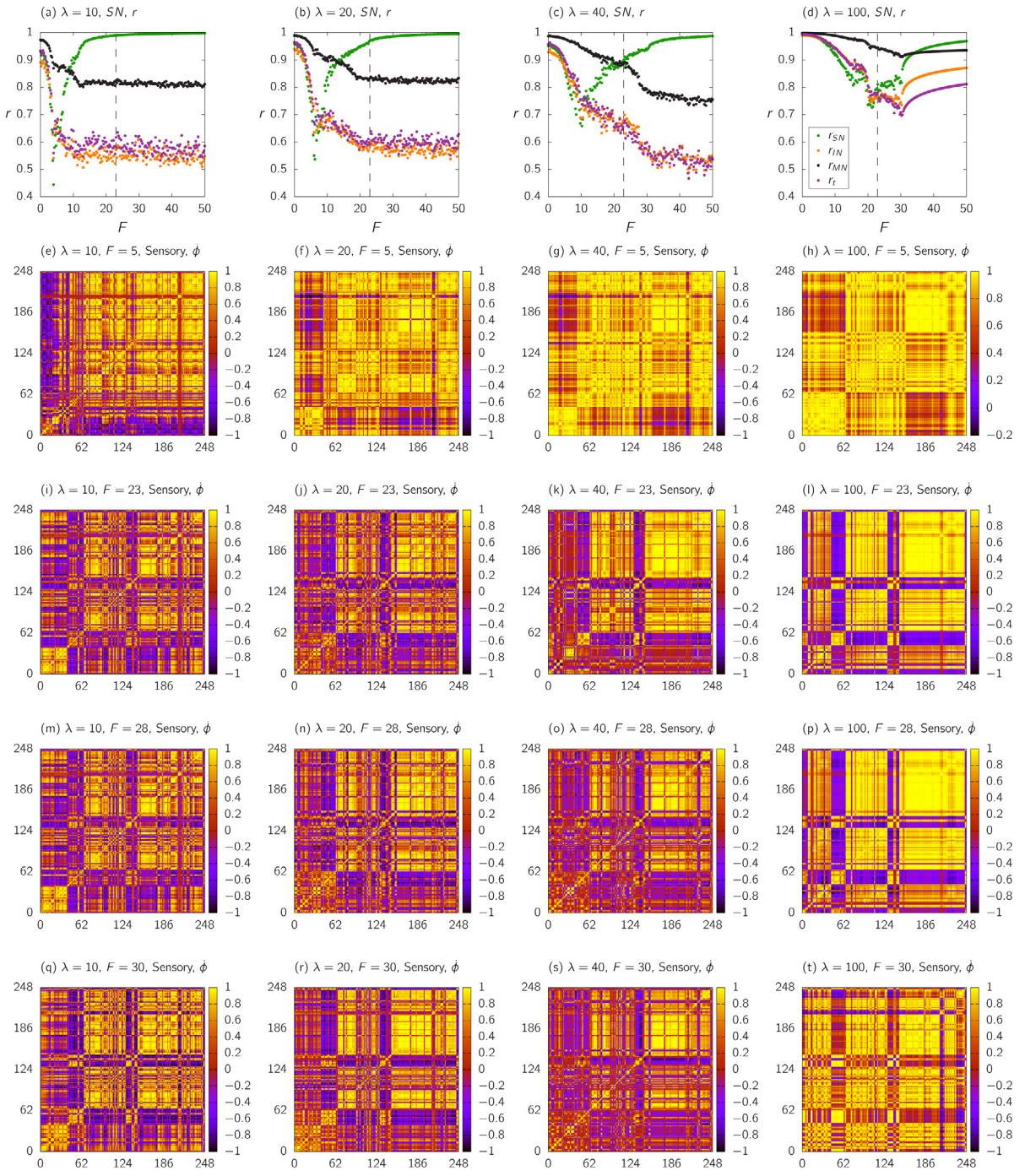

Fig. 6. Panels (a)–(d): the global and local order parameters as a function of the external force F acting on sensory neurons for λ fixed. The dashed lines indicate the critical force, $F_{c,theo}^{SN} = 22.96$. Panels (e)–(t): the velocity–velocity correlation matrix 248×248 obtained using Eq. (11). In each panel, the fixed parameters λ and F are indicated. The sensory neurons (SN) are indexed by 1 to 65, the interneurons (IN) by 66 to 147 and the motoneurons (MN) are indexed by 148 to 248.

correlations identify the three classes reasonably well, although displaying visible internal structure, which indicates a more complex relationship between them. When motoneurons are stimulated (Figs. 10, 11 and table IX of the S.M.) partial synchronization is only possible for very large values of λ and F, but patterns of anti-correlation do appear for small values of λ, similar to what is observed for ganglion G.

In most cases, the order parameters r and $\dot{\psi}$ exhibited a jump near critical force (dashed lines in the plots), which is closer to $F_{c,theo}$ as λ increases. Global and partial synchronization, however, is only observed in some cases and at much larger values of F and λ than predicted by the mean field theory [16]. When the stimulus was applied to ganglion C, in particular, global synchronization happened for $\lambda = 100$ and $F \approx 17$, which is larger than theoretical value found, $F^{C}_{c,theo} = 9.32$.

Previous studies [16] have shown that the Kuramoto model with external localized stimuli leads to global synchronization on synthetic networks with simple topologies, such as random and scale-free, if λ and F are sufficiently large. Here we considered the real neural network of the nematode *C. elegans* and observed full and partial synchronization in very few cases and for higher values of λ and F than predicted. This indicates that the particular modular structure of the network protects the system from 'seizures'. We found that the response of the network is highly complex and depends strongly not only on the stimulated group but also on the intensity F and coupling strength λ. We hypothesize that this complexity reflects the system flexibility to process and differentiate several types of inputs. The group divisions considered here (topological, functional and anatomical) are natural but not exhaustive and finer subdivisions might be important to understand the system response in more detail. Different types of stimuli, such as non-sinusoidal periodic trains or localized pulses, could also bring up interesting responses that might help distinguish the behavior of the different modules.

Acknowledgments

M.A.M.A. acknowledges financial support from CNPq, Brazil (grant 302049/2015-0) and FAPESP, Brazil (grants 2016/06054-3 and 2015/11985-3). C.A.M. was supported by CNPq, Brazil (grant 141021/2017-9).

Appendix A. Supplementary data

Supplementary material related to this article can be found online at https://doi.org/10.1016/j.physa.2019.122051.

References

[1] M.P. van den Heuvel, O. Sporns, Network hubs in the human brain, Trends Cogn. Sci. 17 (2013) 683–696, http://dx.doi.org/10.1016/j.tics.2013.09.012.
[2] M. Rubinov, O. Sporns, Complex network measures of brain connectivity: Uses and interpretations, NeuroImage 52 (2010) 1059–1069, http://dx.doi.org/10.1016/j.neuroimage.2009.10.003.
[3] O. Sporns, R.F. Betzel, Modular brain networks, Annu. Rev. Psychol. 67 (2016) 613–640, http://dx.doi.org/10.1146/annurev-psych-122414-033634.
[4] K.A. Bacik, M.T. Schaub, M. Beguerisse-Diaz, Y.N. Billeh, M. Barahona, Flow-based network analysis of the Caenorhabditis elegans connectome, PLoS Comput. Biol. 12 (2016) 1–27, http://dx.doi.org/10.1371/journal.pcbi.1005055.
[5] C.G. Antonopoulos, Dynamic range in the C. elegans brain network, Chaos 26 (2016) 1–9, http://dx.doi.org/10.1063/1.4939837.
[6] J.S. Kim, M. Kaiser, From Caenorhabditis elegans to the human connectome: a specific modular organization increases metabolic, functional and developmental efficiency, Phil. Trans. R. Soc. Lond. B 369 (2014) 1–9, http://dx.doi.org/10.1098/rstb.2013.0529.
[7] R. Schmidt, K.J.R. LaFleur, M.A. de Reus, L.H. van den Berg, M.P. van den Heuvel, Kuramoto model simulation of neural hubs and dynamic synchrony in the human cerebral connectome, BMC Neurosci. 16 (2015) 1–13, http://dx.doi.org/10.1186/s12868-015-0193-z.
[8] C.M. Gray, Synchronous oscillations in neuronal systems: Mechanisms and functions, J. Comput. Neurosci. 1 (1994) 11–38, http://dx.doi.org/10.1007/BF00962716.
[9] P.J. Uhlhaas, W. Singer, Neural synchrony in brain disorders: Relevance for cognitive dysfunctions and pathophysiology, Neuron 52 (2006) 155–168, http://dx.doi.org/10.1016/j.neuron.2006.09.020.
[10] P. Jiruska, M. de Curtis, J.G.R. Jefferys, C.A. Schevon, S.J. Schiff, K. Schindler, Synchronization and desynchronization in epilepsy: controversies and hypotheses, J. Physiol. 591 (2012) 787–797, http://dx.doi.org/10.1113/jphysiol.2012.239590.
[11] C. Babiloni, R. Lizio, N. Marzano, P. Capotosto, A. Soricelli, A.I. Triggiani, S. Cordone, L. Gesualdo, C. Del Percio, Brain neural synchronization and functional coupling in alzheimer's disease as revealed by resting state EEG rhythms, Int. J. Psychophysiol. 103 (2016) 88–102, http://dx.doi.org/10.1016/j.ijpsycho.2015.02.008.
[12] R.F. Helfrich, B.A. Mander, W.J. Jagust, R.T. Knight, M.P. Walker, Old brains come uncoupled in sleep: Slow wave-spindle synchrony, brain atrophy, and forgetting, Neuron 97 (2018) 221–230, http://dx.doi.org/10.1016/j.neuron.2017.11.020.
[13] J. Sowińska, S.D. Bella, Poor synchronization to the beat may result from deficient auditory-motor mapping, Neuropsychologia 51 (2013) 1952–1963, http://dx.doi.org/10.1016/j.neuropsychologia.2013.06.027.
[14] J. Salmi, U. Roine, E. Glerean, J. Lahnakoski, T. Nieminen-von Wendt, P. Tani, S. Leppämäki, L. Nummenmaa, I.P. Jääskeläinen, S.Carlson, P. Rintahaka, M. Sams, The brains of high functioning autistic individuals do not synchronize with those of others, NeuroImage Clin. 3 (2013) 489–497, http://dx.doi.org/10.1016/j.nicl.2013.10.011.
[15] I. Dinstein, K. Pierce, L. Eyler, S. Solso, R. Malach, M. Behrmann, E. Courchesne, Disrupted neural synchronization in toddlers with autism, Neuron 70 (2011) 1218–1225, http://dx.doi.org/10.1016/j.neuron.2011.04.018.
[16] C.A. Moreira, M.A.M. de Aguiar, Global synchronization of partially forced Kuramoto oscillators on networks, Physica A 514 (2019) 487–496, http://dx.doi.org/10.1016/j.physa.2018.09.096.
[17] S.N. Williams, C.J. Locke, A.L. Braden, K.A. Caldwell, G.A. Caldwell, Epileptic-like convulsions associated with LIS-1 in the cytoskeletal control of neurotransmitter signaling in Caenorhabditis elegans, Hum. Mol. Genet. 13 (2004) 2043–2059, http://dx.doi.org/10.1093/hmg/ddh209.
[18] M.G. Risley, S.P. Kelly, J. Kauliang, B. Grill, K. Dawson-Scully, Modulating behavior in C. elegans using electroshock and antiepileptic drugs, PLoS One 11 (2016) 1–13, http://dx.doi.org/10.1371/journal.pone.0163786.
[19] B.A. Martinez, K.A. Caldwell, G.A. Caldwell, C. elegans as a model system to accelerate discovery for Parkinson disease, Curr. Opin. Genet. Dev. 44 (2017) 102–109, http://dx.doi.org/10.1016/j.gde.2017.02.011.
[20] J.F. Coopera, J.M. Van Raamsdonka, Modeling Parkinson's disease in C. elegans, J. Parkinsons Dis. (2018) 17–32, http://dx.doi.org/10.3233/JPD-171258.

[21] Z.F. WormAtlas, L.A. Altun, C.A. Herndon, C. Wolkow, R. Crocker, D.H. Hall Lints (Eds.), 2002–2018. Available at http://www.wormatlas.org/ (accessed December 2018).
[22] The Open Worm Project. Available at http://openworm.org/ (accessed December 2018).
[23] M. Szalay-Beko, R. Palotai, B. Szappanos, I.A. Kovács, B. Papp, P. Csermely, Moduland plug-in for Cytoscape: determination of hierarchical layers of overlapping network modules and community centrality, Bioinformatics 28 (2012) 2202–2204, http://dx.doi.org/10.1093/bioinformatics/bts352.
[24] I.A. Kovács, R. Palotai, M.S. Szalay, P. Csermely, Community landscapes: An integrative approach to determine overlapping network module hierarchy, identify key nodes and predict network dynamics, PLoS One 5 (2010) 1–14, http://dx.doi.org/10.1371/journal.pone.0012528.
[25] Y. Kuramoto, Self-entrainment of a population of coupled non-linear oscillators, in: International Symposium on Mathematical Problems in Theoretical Physics, Springer-Verlag, Berlin/Heidelberg, 1975, pp. 420–422, http://dx.doi.org/10.1007/BFb0013365.
[26] F.A. Rodrigues, T.K.D.M. Peron, P. Ji, J. Kurths, The Kuramoto model in complex networks, Phys. Rep. 610 (2016) 1–98, http://dx.doi.org/10.1016/j.physrep.2015.10.008.
[27] J.A. Acebrón, L.L. Bonilla, C.J. Pérez, F. Ritort, R. Spigler, The kuramoto model: A simple paradigm for synchronization phenomena, Rev. Modern Phys. 77 (2005) 137–185, http://dx.doi.org/10.1103/RevModPhys.77.137.
[28] A. Arenas, A. Diaz-Guilera, J. Kurths, Y. Moreno, C. Zhou, Synchronization in complex networks, Phys. Rep. 469 (2008) 93–153, http://dx.doi.org/10.1016/j.physrep.2008.09.002.
[29] H. Sakaguchi, Cooperative phenomena in coupled oscillator systems under external fields, Progr. Theoret. Phys. 79 (1988) 39–46, http://dx.doi.org/10.1143/PTP.79.39.
[30] E. Ott, T.M. Antonsen, Low dimensional behavior of large systems of globally coupled oscillators, Chaos 18 (2008) 1–6, http://dx.doi.org/10.1063/1.2930766.
[31] L.M. Childs, S.H. Strogatz, Stability diagram for the forced Kuramoto model, Chaos 18 (2008) 1–9, http://dx.doi.org/10.1063/1.3049136.
[32] M.S. Baptista, F.M.M. Kakmeni, C. Grebogi, Combined effect of chemical and electrical synapses in Hindmarsh-Rose neural networkson synchronization and the rate of information, Phys. Rev. E 82 (2010) 1–12, http://dx.doi.org/10.1103/PhysRevE.82.036203.
[33] C.G. Antonopoulos, S. Srivastava, S.E.S. Pinto, M.S. Baptista, Do brain networks evolve by maximizing their information flow capacity? PLoS Comput. Biol. 11 (2015) 1–29, http://dx.doi.org/10.1371/journal.pcbi.1004372.
[34] R.R. Borges, F.S. Borges, E.L. Lameu, A.M. Batista, K.C. Iarosz, I.L. Caldas, C.G. Antonopoulos, M.S. Baptista, Spike timing-dependent plasticity induces non-trivial topology in the brain, Neural Netw. 88 (2017) 58–64, http://dx.doi.org/10.1016/j.neunet.2017.01.010.
[35] A. Fortunato, Community detection in graphs, Phys. Rep. 486 (2010) 75–174, http://dx.doi.org/10.1016/j.physrep.2009.11.002.
[36] M. Newman, M. Girvan, Finding and evaluating community structure in networks, Phys. Rev. E 69 (2004) 1–15, http://dx.doi.org/10.1103/PhysRevE.69.026113.
[37] M. Newman, Finding community structure in networks using the eigenvectors of matrices, Phys. Rev. E 74 (2006) 1–19, http://dx.doi.org/10.1103/PhysRevE.74.036104.
[38] P. Shannon, A. Markiel, O. Ozier, N.S. Baliga, J.T. Wang, D. Ramage, N. Amin, B. Schwikowski, T. IdekeR, Cytoscape: a software environment for integrated models of biomolecular interaction networks, Genome Res. 3 (2003) 2498–2504, http://dx.doi.org/10.1101/gr.1239303.
[39] Y. Sohn, M.K. Choi, Y.Y. Ahn, J. Lee, J. Jeong, Topological cluster analysis reveals the systemic organization of the Caenorhabditis elegans connectome, PLoS Biol. 7 (2011) 1–10, http://dx.doi.org/10.1371/journal.pcbi.1001139.
[40] R.K. Pan, N. Chatterjee, S. Sinha, Mesoscopic organization reveals the constraints governing Caenorhabditis elegans nervous system, PLoS One 5 (2010) 1–15, http://dx.doi.org/10.1371/journal.pone.0009240.
[41] L.R. Varshney, B.L. Chen, E. Paniagua, D.H. Hall, D.B. Chklovskii, Structural properties of the Caenorhabditis elegans neuronal network, PLoS Comput. Biol. 7 (2011) 1–21, http://dx.doi.org/10.1371/journal.pcbi.1001066.
[42] G. Yan, P.E. Vértes, E.K. Towlson, Y.L. Chew, D.S. Walker, W.R. Schafer, A.-L. Barabási, Network control principles predict neuron function in the Caenorhabditis elegans connectome, Nature 550 (2017) 519–523, http://dx.doi.org/10.1038/nature24056.
[43] R. Brette, Computing with neural synchrony, PLoS Comput. Biol. 8 (2012) 1–18, http://dx.doi.org/10.1371/journal.pcbi.1002561.
[44] W.M. Usrey, R.C. Reid, Synchronous activity in the visual system, Annu. Rev. Physiol. 61 (1999) 435–456, http://dx.doi.org/10.1146/annurev.physiol.61.1.435.
[45] E. Salinas, T.J. Sejnowski, Correlated neuronal activity and the flow of neural information, Nat. Rev. Neurosci. 2 (2001) 539–550, http://dx.doi.org/10.1038/35086012.
[46] I.H. Brivanlou, D.K. Warland, M. Meister, Mechanisms of concerted firing among retinal ganglion cells, Neuron 20 (1998) 527–539, http://dx.doi.org/10.1016/S0896-6273(00)80992-7.
[47] M. Meister, M.J. Berry, The neural code of the retina, Neuron 22 (1999) 435–450, http://dx.doi.org/10.1016/S0896-6273(00)80700-X.
[48] T. Gollisch, M. Meister, Rapid neural coding in the retina with relative spike latencies, Science 319 (2008) 1108–1111, http://dx.doi.org/10.1126/science.1149639.
[49] P.X. Joris, L.H. Carney, P.H. Smith, T.C. Yin, Enhancement of neural synchronization in the anteroventral cochlear nucleus. I. Responses to tones at the characteristic frequency, J. Neurophysiol. 71 (1994) 1022–1036, http://dx.doi.org/10.1152/jn.1994.71.3.1022.
[50] P.X. Joris, P.H. Smith, T.C. Yin, Coincidence detection in the auditory system: 50 years after Jeffress, Neuron 21 (1998) 1235–1238, http://dx.doi.org/10.1016/S0896-6273(00)80643-1.
[51] A. Arenas, A. Fernández, S. Gómez, A complex network approach to the determination of functional groups in the neural system of C. elegans, in: P. Lió, E. Yoneki, J. Crowcroft, D.C. Verma (Eds.), Bio-Inspired Computing and Communication (2008), in: Bio-Inspired Computing and Communication. BIOWIRE 2007. Lecture Notes in Computer Science, vol. 5151, Springer, Berlin, Heidelberg, http://dx.doi.org/10.1007/978-3-540-92191-2_2.